

Article

Condensation of an Azeotropic Mixture inside 2.5 mm ID Minutubes

Andrea Diani and Luisa Rossetto *

Department of Industrial Engineering, University of Padova, via Venezia 1, 35131 Padova, Italy;
andrea.diani@unipd.it

* Correspondence: luisa.rossetto@unipd.it; Tel.: +39-049-827-6869

Received: 31 August 2020; Accepted: 30 September 2020; Published: 2 October 2020



Abstract: The ongoing miniaturization of air conditioning and refrigeration systems, in order to limit, as much as possible, the refrigerant charge, calls for smaller and smaller heat exchangers. Besides, the new environmental regulations are calling for new pure refrigerants or refrigerants mixtures with lower values of global warming potentials (GWPs). In this context, this paper analyzes the possible implementation of minutubes during condensation of the azeotropic mixture R513A. Two minutubes are tested: a smooth tube with an inner diameter of 2.5 mm, and a microfin tube with an inner diameter at the fin tip of 2.4 mm. The effects of vapor quality (varied in the range 0.10–0.99), of mass velocity (varied in the range 200–1000 kg m⁻² s⁻¹), and of saturation temperature (30 °C and 40 °C) on the heat transfer coefficient are investigated. The experimental results indicate that the heat transfer coefficient increases as both vapor quality and mass velocity increase, both in the case of the smooth tube and of the microfin tube, but the slope of the heat transfer coefficient trend respect to vapor quality is higher in the case of the microfin tube. The microfin tube shows, on average, heat transfer coefficients are 79% higher than those of the smooth tube under the same working conditions. Since R513A is a possible substitute of R134a, some experimental data during condensation heat transfer are also compared against those for R134a. Finally, the experimental results are compared against values estimated by empirical correlations available in the open literature.

Keywords: condensation; R513A; heat transfer coefficient; smooth tube; microfin tube

1. Introduction

R513A is an azeotropic mixture made of R1234yf and R134a (0.56/0.44 by mass). R1234yf is an HydroFluroOlefin with a Global Warming Potential lower than 1 [1], and it is placed in the A2L flammability class. R134a is among the most used HydroFluroCarbons, not flammable (A1 flammability class), widely implemented in existing air conditioning systems, but it must be phased out in a near future due to its high GWP, which is 1430. Therefore, the presence of R134a makes the mixture not flammable, whereas the presence of R1234yf lowers the warming impact of the mixture. Coupled with small sized tubes, R513A could be a viable solution for the next generation of air conditioning equipment.

R32 and R134a local heat transfer coefficients were measured by Matkovic et al. [2]. Experimental tests were carried out at 40 °C saturation temperature inside a 0.96 mm ID circular minutube for mass velocities in the range 100–1200 kg m⁻² s⁻¹. The heat transfer coefficient increased with mass velocity and vapor quality; therefore, condensation was shear stress dominated, except some data at 100 and 200 kg m⁻² s⁻¹, which overlapped in the graph.

Zhang et al. [3] experimentally investigated the condensation of R22, R410A, and R407C inside two stainless steel tubes with inner diameters of 1.088 mm and 1.289 mm. Tests were run for mass velocities in the range 300–600 kg m⁻² s⁻¹, for saturation temperatures of 30 °C and 40 °C. The experimental

results indicated that the condensation heat transfer coefficient increases with mass velocity and vapor quality, increasing more rapidly in the high vapor quality region.

More recently, Guo et al. [4] obtained heat transfer coefficients during the condensation of R1234ze(E), R290, R161, and R41 in a smooth horizontal tube with an inner diameter of 2 mm. Mass velocity was varied from 200 to 400 kg m⁻² s⁻¹, and saturation temperature from 35 °C to 40 °C. The experimental results showed that the heat transfer coefficient increases as vapor quality and mass velocity increase, and as saturation temperature decreases. Other works related to condensation in minichannels can be found in [5–7].

Adding microfins on the inner circumference of the tube has proven to enhance the two-phase heat transfer. Small-sized microfin tubes were initially studied for applications that involve carbon dioxide, due to its high working pressure [8–10]. Considering microfin tubes classified as minitubes, i.e., with diameters ranging between 1 and 3 mm [11], just a few studies investigated refrigerants' two-phase heat transfer. Experimental measurements of the heat transfer coefficient were carried out by Diani et al. [12], who studied R1234yf and R1234ze(E) condensing inside a 2.4 mm ID microfin tube. Mass velocities were varied from 300 to 1000 kg m⁻² s⁻¹, for saturation temperatures of 30 °C and 40 °C. R1234ze(E) and R134a showed similar values of heat transfer coefficients, whereas R1234yf showed lower values.

Bashar et al. [13] investigated the condensation heat transfer of R134a flowing inside a microfin tube having an equivalent diameter of 2.17 mm and inside a smooth tube with an inner diameter of 2.14 mm. Data were measured for mass velocities from 50 to 300 kg m⁻² s⁻¹, and saturation temperatures from 20 °C to 30 °C. The heat transfer coefficient was higher in the case of the microfin tube for all the investigated mass fluxes and, considering the mass velocity 100 kg m⁻² s⁻¹, it was 2–5 times greater than that of the smooth tube.

Diani et al. [14] conducted experiments during R1234yf flow boiling inside a microfin tube with an outer diameter of 3.0 mm, for mass fluxes from 375 to 940 kg m⁻² s⁻¹, heat fluxes from 10 kW m⁻² to 50 kW m⁻², with a saturation temperature at the inlet of the test section of 30 °C. The experimental results showed that the flow boiling phenomenon is controlled by nucleate boiling, especially at low vapor qualities, and by convective boiling, especially at high vapor qualities.

Jige and Inoue [15] investigated R32 flow boiling inside microfin tubes with equivalent diameters of 2.1 mm, 2.6 mm, and 3.1 mm. Mass velocity was varied from 50 to 200 kg m⁻² s⁻¹ and heat flux from 5 to 40 kW m⁻². The saturation temperature was 15 °C. The effect of tube diameter on the flow boiling heat transfer coefficient was more appreciable at higher vapor quality and lower mass velocity (the lower the tube diameter, the higher the heat transfer coefficient). Frictional pressure drops were highly affected by tube diameter: the lower the tube diameter, the higher the pressure drop.

Hirose et al. [16] studied R1234ze(E) condensation inside three different microfin tubes with the same outer diameter of 4 mm. The effects of fin parameters, i.e., of helix angle, fin height, and fin number were analyzed for mass velocities in the range 50–400 kg m⁻² s⁻¹, at a saturation temperature of 35 °C.

There are many candidates to replace R134a. Some of them are pure fluids, such as R1234ze(E) and R1234yf; others are azeotropic mixtures, such as R513A, R515A and R516A; others are zeotropic mixtures, such as R450A, R445A, R430A, R436A, and R456A. Heredia-Aricapa et al. [17] overviewed possible refrigerants mixtures as replacements of common HFCs like R134a, R404A, and R410A. Among the replacements of R134a, they identified R445A, R430A, R515A, R436A, R456A, and R515A. R436A and R430A are the alternatives with the greatest differences in the thermophysical properties, due to the presence of hydrocarbons in the mixtures. The comparison among fluids was given in terms of COP and cooling capacity in a vapor compression system.

Kedzierski et al. [18] carried out experimental tests during pool boiling on a reentrant cavity surface for R134a, R1234yf, R513A, and R450A. At constant wall superheat and pressure, with a saturation temperature of 277.6 K, the heat flux for R1234yf and R513A was, on average, 16% and 19% less than that for R134a, respectively, for heat fluxes between 20 kW m⁻² and 110 kW m⁻², whereas the

heat flux for R450A was, on average, 57% less than that of R134a for heat fluxes between 30 kW m^{-2} and 110 kW m^{-2} . Other works related to R513A can be found in Diani et al. [19,20], but no comparisons with R134a were reported.

Being a relatively new mixture, to date, no work about R513A condensation inside mini microfin tubes with diameters lower than 3 mm can be found in the open literature. Two minitubes are tested in this research: the first one is a smooth tube with an inner diameter of 2.5 mm, and the second one is a microfin tube with an inner diameter at the fin tip of 2.4 mm. This work is aimed at enlarging the experimental database of heat transfer coefficients during R513A condensation inside smooth and microfinned minitubes. The wide range of operative conditions will permit us to understand how each working parameter, i.e., vapor quality, mass velocity, and saturation temperature, affects the two-phase heat transfer both in the case of the smooth tube and of the microfin tube, highlighting the differences among the two tubes. Finally, the experimental condensation heat transfer coefficients will be compared against values estimated by empirical correlations.

2. Experimental Facility and Test Sections

The experimental facility is in the Laboratory of Heat Transfer in MicroGeometries at the Department of Industrial Engineering of University of Padova, Italy. Figure 1 shows a schematic of the liquid pumped circuit. A magnetically coupled gear pump was chosen to avoid any possible oil traces in the refrigerant. The pump circulates the refrigerant into a Coriolis effect mass flowmeter, which presents a reading accuracy of $\pm 0.1\%$. The refrigerant enters an evaporator in subcooled conditions, and it exits in superheated conditions. The evaporator is a BPHE where refrigerant flows in countercurrent with hot water, supplied in the hot water loop. An electric boiler, regulated with a PID controller, guarantees an inlet water temperature of $60 \text{ }^\circ\text{C}$. A tube-in-tube pre-condenser is aimed at partially condensing the superheated vapor, which flows in the inner tube. Cold water, supplied by a water-cooled stabilized chiller, flows in the annulus. The chiller permits to set the temperature of the water at the inlet of the pre-condenser. In addition, a valve permits variation in the water flow rate, and therefore it is possible to adjust the heat flow rate exchanged in the pre-condenser to set the refrigerant conditions at the inlet of the test section. The refrigerant partially condenses in the test section, and it is later fully condensed and subcooled in the post-condenser, which is another BPHE. In this case, the refrigerant flows in counter current with a mixture of water/glycol supplied by an air-cooled chiller. The refrigerant passes through a drier filter prior to re-enter into the pump. The saturation conditions are controlled by means of a damper, which is connected to the air pressure line.

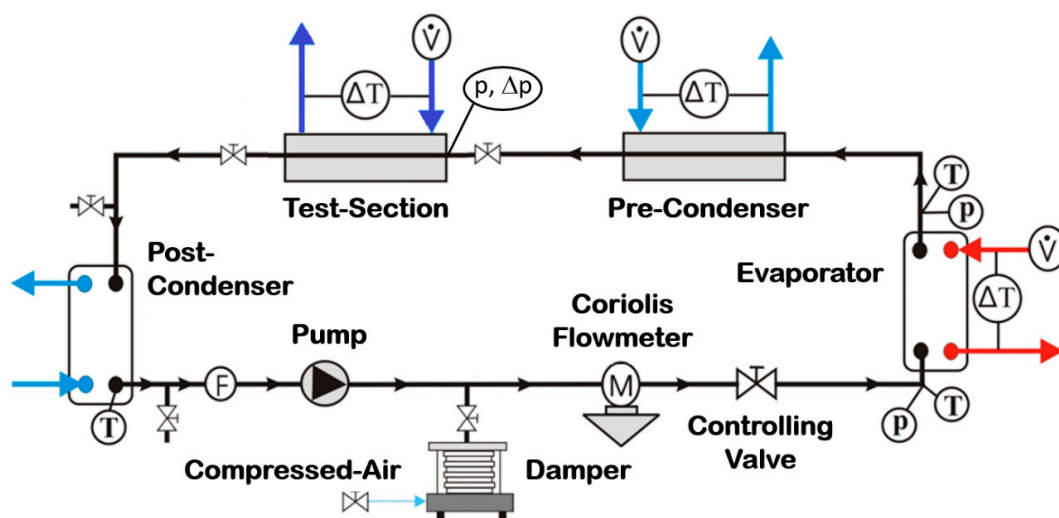


Figure 1. Schematic of the test rig.

As depicted in Figure 1, temperatures (measured by T-type thermocouples with an accuracy of ± 0.05 K) and pressures of the refrigerant (measured by absolute pressure transducers with an accuracy of ± 1950 Pa) are measured in several locations throughout the circuit, so it is possible to determine its thermodynamic state. The refrigerant conditions at the inlet of the test section, i.e., at the exit of the pre-condenser, derive from an energy balance at the pre-condenser, as will be explained in the next section. The water flow rate in the cold-water loop at the pre-condenser, necessary for the energy balance, is measured by a magnetic flowmeter, with a reading accuracy of $\pm 0.25\%$. The water temperature difference at the pre-condenser is measured by a T-type thermopile, which has an accuracy of ± 0.03 K.

Two different minitubes made of copper were tested. The first one is a smooth tube with an internal diameter of 2.5 mm and an outer diameter of 4.5 mm. The second one is a microfin tube with an inner diameter at the fin tip of 2.4 mm, an outer diameter of 3.0 mm, having 40 fins, and each fin has a height of 0.12 mm and an apex angle of 43° ; the helix angle is 7° . Both the test section for the smooth tube and the one for the microfin tube are composed of the tested tube, which is horizontally located, around which a 1.9 mm ID smooth tube is wrapped. Cold water, supplied by a thermostatic bath and measured by a magnetic flowmeter with an accuracy of $\pm 0.50\%$ of the reading, flows in the wrapped tube, to remove the heat flow rate necessary for the condensation of the refrigerant flowing inside the horizontally located tested tube. Two curves, one at the inlet and another at the outlet, permit to host two T-type thermocouples (accuracy ± 0.05 K), which measure the water inlet and outlet temperatures in the test section. On the external wall of the tested tubes, T-type thermocouples were glued to measure the wall temperature. Figure 2 shows a schematic, as well as the geometrical dimensions, of the test section for the smooth tube. The blue dots represent the thermocouples which measure the water temperatures, whereas the red dots represent the thermocouples attached on the external wall of the tested tube. The tested tubes with the wrapped tubes were finally inserted inside an aluminum housing with a U-shape. This housing was filled with an alloy of tin/lead, which was casted inside. This alloy is needed to have a good thermal contact between the wrapped tube, inside which the cold water flows, and the tested tube, inside which the refrigerant condenses. AF/Armaflex was used as thermal insulation around the test section to limit the heat losses through the external ambient. Pressure ports were soldered downstream and upstream of the test sections: the upstream pressure port is connected to an absolute pressure transducer (accuracy of ± 1950 Pa), whereas both upstream and downstream pressure ports are connected to a differential pressure transducer (accuracy of ± 25 Pa).

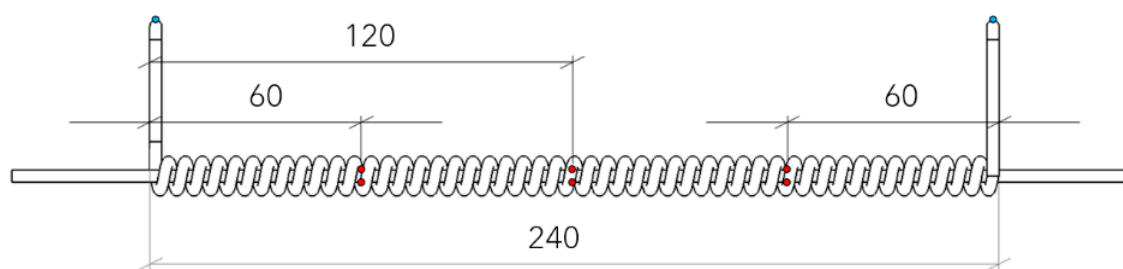


Figure 2. Schematic of the test section for the 2.5 mm ID smooth tube.

3. Data Analysis

The vapor quality at the inlet of the test section, $h_{TS,in}$, can be extrapolated from the specific enthalpy at the exit of the pre-condenser, $h_{PC,out}$, calculated as:

$$h_{TS,in} = h_{PC,out} = h_{vs} - \frac{\dot{m}_{w,PC} \cdot c_{p,w} \cdot \Delta T_{w,PC}}{\dot{m}_{ref}} \quad (1)$$

where h_{vs} is the specific enthalpy of the refrigerant in superheated vapor conditions at the exit of the evaporator, which is calculated from the knowledge of its temperature and pressure. $\dot{m}_{w,pc}$ is the mass flow rate of the water flowing in the pre-condenser, $c_{p,w}$ is the water specific heat, $\Delta T_{w,pc}$ is the water temperature difference between outlet and inlet of the pre-condenser, and \dot{m}_{ref} is the refrigerant mass flow rate. The inlet vapor quality can be calculated from the knowledge of $h_{TS,in}$ as:

$$x_{in} = \frac{h_{TS,in} - h_L}{h_V - h_L} \quad (2)$$

where h_V and h_L are the specific enthalpies of saturated vapor and liquid, respectively, calculated from the inlet pressure. REFPROP 10 (Lemmon et al. [21]) was used to calculate all the refrigerant thermodynamic properties, since it implements updated equations for R513A.

In a similar way, the refrigerant specific enthalpy at the outlet of the test section, $h_{TS,out}$, can be derived from an energy balance, as:

$$h_{TS,out} = h_{TS,in} - \frac{q_{w,TS}}{\dot{m}_{ref}} = h_{TS,in} - \frac{\dot{m}_{w,TS} \cdot c_{p,w} \cdot (t_{w,TS,out} - t_{w,TS,in})}{\dot{m}_{ref}} \quad (3)$$

where $q_{w,TS}$ is the heat flow rate calculated in the water side, and, in this case, $\dot{m}_{w,TS}$ is the mass flow rate of the water flowing in the test section, $t_{w,TS,out}$ and $t_{w,TS,in}$ are the water temperature at the outlet and inlet of the test section, respectively. Once $h_{TS,out}$ is known, the outlet vapor quality is calculated as:

$$x_{out} = \frac{h_{TS,out} - h_L}{h_V - h_L} \quad (4)$$

where h_V and h_L are the specific enthalpy of saturated vapor and liquid, respectively, calculated at the outlet pressure. Experimental results, discussed in the next section, will be referred to the mean vapor quality, which is the arithmetic average between inlet vapor quality and outlet vapor quality.

The experimental tests permitted to calculate, both for the smooth tube and for the microfin tube, the heat transfer coefficient (HTC), as:

$$HTC = \frac{q_{w,TS}}{A_D \cdot (\bar{t}_{sat} - \bar{t}_{wall})} \quad (5)$$

where \bar{t}_{sat} and \bar{t}_{wall} are the mean saturation and wall temperatures. A_D is equal to the inner surface area in the case of the smooth tube, whereas it is equal to the inner surface area of an equivalent smooth with the inner diameter at the fin tip in the case of the microfin tube.

Following the procedure suggested by Kline and McClinton [22], considering a level of confidence of 95%, the mean uncertainty on the heat transfer coefficient is $\pm 4.2\%$, whereas on the mean vapor quality is ± 0.027 .

4. Experimental Results

4.1. Smooth Tube

4.1.1. Single-Phase Results

The test section developed for the smooth tube was first verified during single phase flow involving the forced convection of subcooled liquid. The main purposes of these tests were to check the heat flow rate calculated on the water side and the one on the refrigerant side and to verify if the measuring technique was suitable by calculating the single phase heat transfer coefficients and by comparing these results against values predicted by well-known correlations from the literature.

These tests were run with an inlet subcooling level between 17 K and 21 K, at a pressure of about 11.5 bar, for mass velocities from 400 to 1000 kg m⁻² s⁻¹. Mass velocity is defined as:

$$G = \frac{4 \cdot \dot{m}_{ref}}{\pi \cdot D_i^2} \quad (6)$$

where D_i is the inner diameter. The heat transfer coefficient can be calculated as in Equation (5) but in this case, \bar{t}_{ref} is used instead of \bar{t}_{sat} . Two T-type thermocouples, downstream and upstream of the test section, were used to measure the inlet and outlet refrigerant temperatures.

The experimental results demonstrate that the heat flow rates calculated on the water side and on the refrigerant side are, on average, within $\pm 4\%$. Figure 3 reports the heat transfer coefficients plotted against the mass velocity. As expected, the heat transfer coefficient increases as the mass velocity increases. Figure 3 also reports the comparison between the experimental values and the values predicted by the correlations of Dittus and Boelter [23] and of Petukhov and Popov [24]. The correlation of Petukhov and Popov [24] aptly predicts the experimental values, with a relative deviation of 3.9%, an absolute deviation of 4.0% and a standard deviation of 4.0%. The correlation of Dittus and Boelter [23] shows a relative deviation of -0.9% , an absolute deviation of 7.8% and a standard deviation of 9.1%.

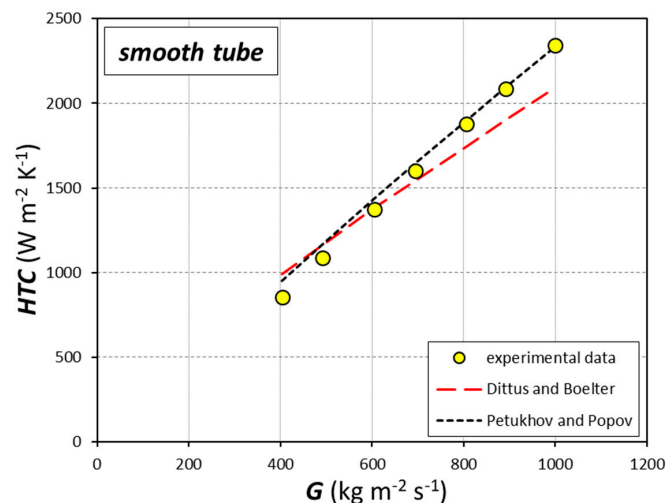


Figure 3. Single-phase heat transfer coefficient for the smooth tube vs. mass velocity. Experimental data and estimations by Dittus and Boelter [23] and by Petukhov and Popov [24].

Therefore, since the percentage difference between heat flow rate on the refrigerant side and the one on the water side is within $\pm 4\%$, and since empirical correlations taken from the literature are able to estimate the experimental values of liquid-phase heat transfer coefficients, the test section for the 2.5 mm ID smooth tube is deemed to be verified.

4.1.2. Condensation Results

The operating conditions during the condensing tests for the 2.5 mm ID smooth tube are the following: mass velocity in the range 200–1000 kg m⁻² s⁻¹ and saturation temperature at the inlet of 30 °C and 40 °C. Experimental tests involve partial condensation inside the test tube, with a vapor quality difference between inlet and outlet from 0.08 to 0.40, depending on the mass velocity. Therefore, in order to investigate vapor qualities from 0.1 to 0.99, tests were run by varying the inlet vapor quality.

The collected heat transfer coefficients during condensation inside the smooth tube at a saturation temperature at the inlet of the test section of 40 °C are reported in Figure 4. Only data which involve an exchanged heat flow rate higher than 30 W are reported, in order to avoid data with high uncertainties. Data are plotted against the mean vapor quality in the test section at different mass velocities. A clear

effect of both mass velocity and vapor quality is visible: the higher the mass velocity and the vapor quality, the higher the heat transfer coefficient, due to the diminishing liquid film thickness. According to the flow regime map developed by Doretti et al. [25] and reported by Cavallini et al. [26], all the experimental data fall in the ΔT -independent zone, i.e., annular flow, except data at $G = 200 \text{ kg m}^{-2} \text{ s}^{-1}$ up to a mean vapor quality of 0.5, which fall into the ΔT -dependent zone, i.e., they are in stratified flow regime. Data at higher mass velocity shows a higher slope of the heat transfer coefficient trend, highlighting a higher convective effect as the mass velocity increases.

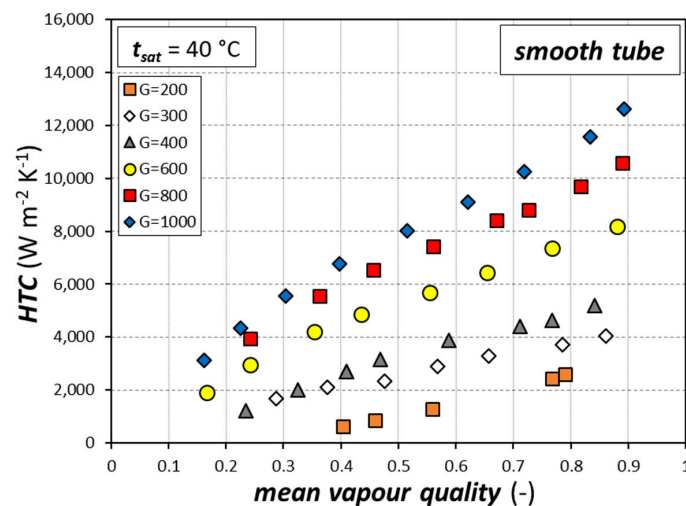


Figure 4. Heat transfer coefficient during condensation for the smooth tube vs. mean vapor quality at $t_{sat} = 40 \text{ °C}$. G expressed in $[\text{kg m}^{-2} \text{ s}^{-1}]$.

Figure 5 reports the data collected during condensation inside the smooth tube for a saturation temperature at the inlet of the test section of 30 °C . All these data fall in the ΔT -independent zone and, as a result, the heat transfer coefficient increases as both the vapor quality and mass velocity increase. The comparison with Figure 4 reveals the effect of the saturation temperature. A higher saturation temperature implies a higher vapor density; thus, at constant mass velocity, it also implies a lower vapor velocity, with consequent lower convective effects. This aspect can be observed in the heat transfer coefficients reported in Figures 4 and 5: the heat transfer coefficient tends to decrease as the saturation temperature increases, due to lower convective effects.

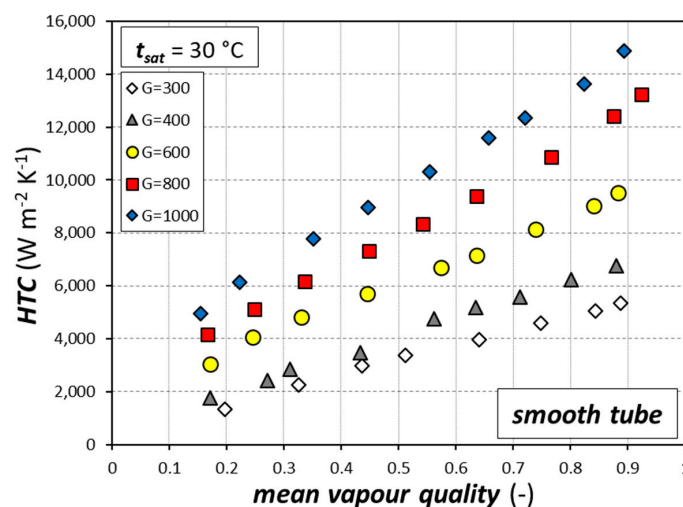


Figure 5. Heat transfer coefficient during condensation for the smooth tube vs. mean vapor quality at $t_{sat} = 30 \text{ °C}$. G expressed in $[\text{kg m}^{-2} \text{ s}^{-1}]$.

4.2. Microfin Tube

4.2.1. Single-Phase Results

In a similar way to the validation procedure depicted in Section 4.1.1, single-phase tests were carried out during R1234yf liquid flow to validate the test section for the 2.4 mm ID microfin tube, and the experimental results revealed that the heat flow rate calculated on the water side was within ± 1.5 W the one on the refrigerant side, and that the experimental single-phase heat transfer coefficients were aptly estimated by empirical correlations from the literature. Therefore, the test section for the microfin tube was deemed verified. More details can be found in Diani et al. [12].

4.2.2. Condensation Results

The operating conditions during the condensing tests for the 2.4 mm ID microfin tube are the following: mass velocity in the range $200\text{--}1000\text{ kg m}^{-2}\text{ s}^{-1}$, saturation temperature at the inlet of $30\text{ }^{\circ}\text{C}$ and $40\text{ }^{\circ}\text{C}$. In this case, the mass velocity is calculated as reported in Equation (6) but the inner diameter at the fin tip is used as D_i .

Figure 6 shows the condensation heat transfer coefficients plotted against the mean vapor quality for the microfin tube with a saturation temperature at the inlet of the test section of $40\text{ }^{\circ}\text{C}$. Again, only data which involve an exchanged heat flow rate higher than 30 W are reported. According to the flow regime map developed by Doretto et al. [25] and reported by Cavallini et al. [26], all the experimental data fall in the annular flow regime. Therefore, the higher the vapor quality and mass velocity, the higher the heat transfer coefficient will be. Compared to the results during condensation inside the smooth tube reported in Figure 4, the condensation heat transfer coefficients for the microfin tube are higher, and the comparison reveals that data at mass velocities of $200, 300,$ and $400\text{ kg m}^{-2}\text{ s}^{-1}$ are particularly enhanced. Indeed, the slope of the heat transfer coefficients with mean vapor quality is now much higher for these low mass velocities: taking for instance $G = 400\text{ kg m}^{-2}\text{ s}^{-1}$, the heat transfer coefficient passes from approximately $2000\text{ W m}^{-2}\text{ K}^{-1}$ at $x_{mean} = 0.3$ to a value of about $5000\text{ W m}^{-2}\text{ K}^{-1}$ at $x_{mean} = 0.8$ for the smooth tube, i.e., it is 2.5 times higher, whereas it passes from approximately $3500\text{ W m}^{-2}\text{ K}^{-1}$ at $x_{mean} = 0.3$ to a value of about $12500\text{ W m}^{-2}\text{ K}^{-1}$ at $x_{mean} = 0.8$ for the microfin tube, i.e., it is 3.5 times higher.

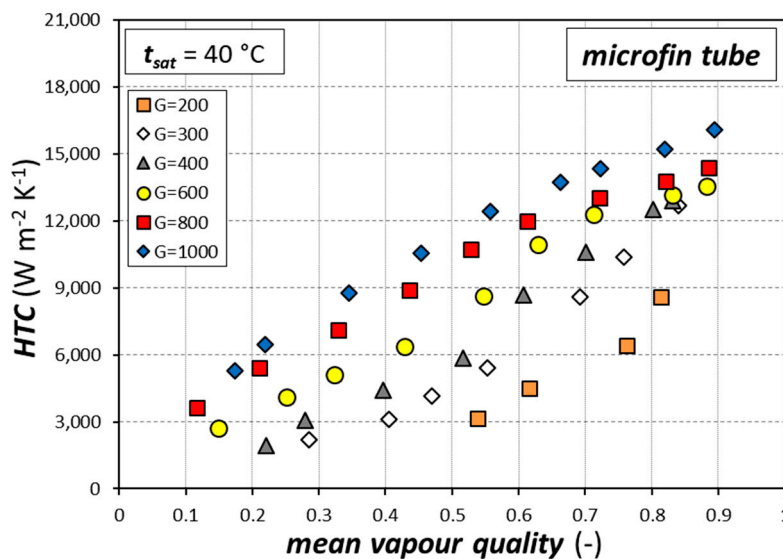


Figure 6. Heat transfer coefficient during condensation for the microfin tube vs. mean vapor quality at $t_{sat} = 40\text{ }^{\circ}\text{C}$. G expressed in $[\text{kg m}^{-2}\text{ s}^{-1}]$.

Results with an imposed saturation temperature at the inlet of the test section of 30 °C for the microfin tube are reported in Figure 7. Again, all the experimental data fall in the annular flow regime, and the heat transfer coefficient increases with mass velocity and vapor quality. The comparison with Figure 6 reveals the effect of saturation temperature: as stated for the smooth tube, the higher the saturation temperature, the lower the heat transfer coefficient, due to lower convective effects that result from the lower vapor velocity.

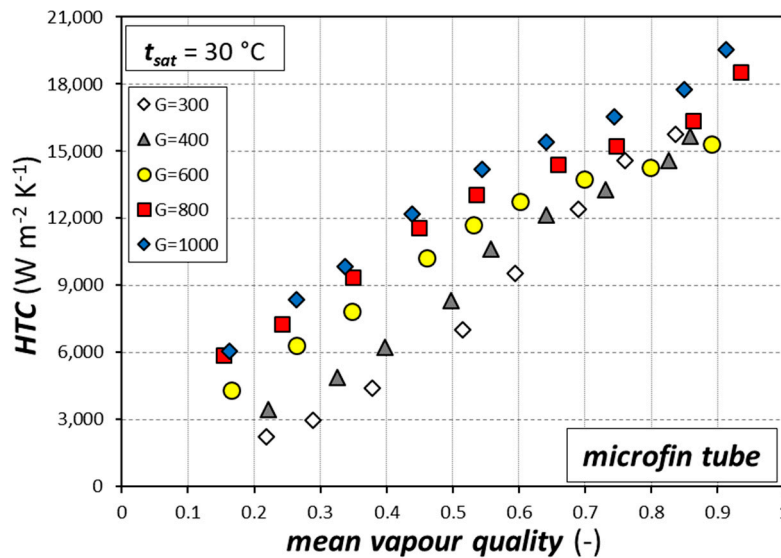


Figure 7. Heat transfer coefficient during condensation for the microfin tube vs. mean vapor quality at $t_{sat} = 30\text{ °C}$. G expressed in $[\text{kg m}^{-2}\text{ s}^{-1}]$.

4.3. Comparison among the Tubes

The heat transfer coefficients of smooth tube and microfin tube are here compared under the same working conditions. To better explain the comparison, the parameter called the Enhancement Factor (EF) is introduced:

$$EF = \frac{HTC_{microfin}}{HTC_{smooth}} \tag{7}$$

where $HTC_{microfin}$ and HTC_{smooth} represent the heat transfer coefficient of the microfin tube and of the smooth tube, respectively, under the same operative conditions.

The Enhancement Factor is plotted versus the mean vapor quality in Figure 8, considering a saturation temperature of 40 °C. Adding microfins on the internal area of the microfin tube improves the thermal behavior during condensation; indeed, the EF is always higher than 1. In addition, the benefits of the microfins increase as mass velocity decreases, i.e., the highest EF is shown at the lowest mass velocities. At these lowest mass velocities, the EF increases along with the increasing vapor quality. Similar conclusions are made at $t_{sat} = 30\text{ °C}$.

The area enhancement ratio, i.e., the ratio between the total inner surface area of the microfin tube and the inner surface of a smooth tube having the fin tip diameter as inner diameter, is 1.89. It is worth highlighting that, at $G = 300$ and $400\text{ kg m}^{-2}\text{ s}^{-1}$ for mean vapor qualities higher than 0.4, the EF is higher than the mere increase of the heat transfer area, and thus the microfins have a positive effect on the heat transfer especially at low mass velocities, increasing the turbulence of the liquid film. Considering all the experimental data, the average Enhancement Factor is 1.79.

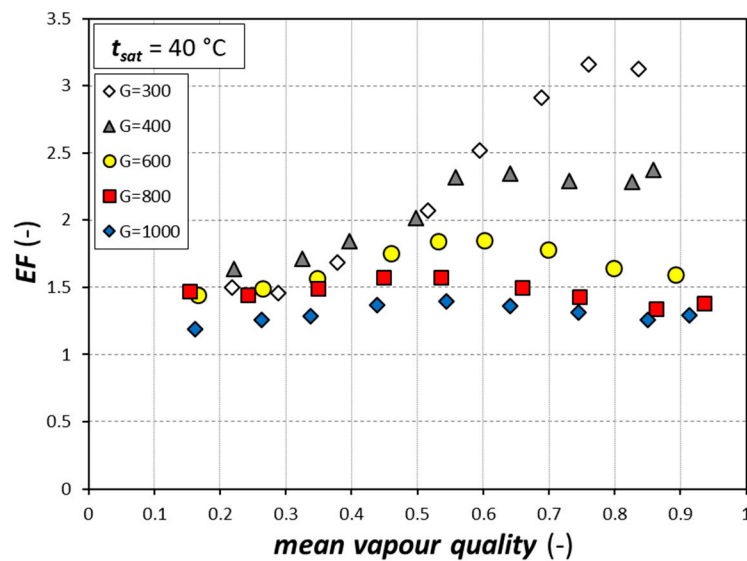


Figure 8. Enhancement Factor (EF) vs. mean vapor quality at $t_{sat} = 40\text{ °C}$. G expressed in $[\text{kg m}^{-2} \text{s}^{-1}]$.

4.4. Comparison among Refrigerants

Being one of the possible direct drop in replacements of R134a in the near future, the performance of R513A is compared against that of R134a. Heat transfer coefficients during R134a condensation inside a microfin tube with an inner diameter at the fin tip of 2.4 mm are borrowed by Diani et al. [12]. The comparison can start by comparing the different thermophysical and transport properties of the two fluids. Table 1 reports the main properties of R134a and R513A.

Table 1. Thermophysical and transport properties of R134a and R513A. Values from REFPROP 10 (Lemmon et al. [21]).

Properties	R134a	R513A
t_{sat} [°C]	30	30
p_{sat} [bar]	7.702	8.211
ρ_L [kg m^{-3}]	1188	1115
ρ_V [kg m^{-3}]	37.54	43.50
λ_L [$\text{W m}^{-1} \text{K}^{-1}$]	0.079	0.068
λ_V [$\text{W m}^{-1} \text{K}^{-1}$]	0.014	0.015
μ_L [$\mu\text{Pa s}$]	183	156
μ_V [$\mu\text{Pa s}$]	11.9	11.8
$c_{p,L}$ [$\text{J kg}^{-1} \text{K}^{-1}$]	1447	1436
$c_{p,V}$ [$\text{J kg}^{-1} \text{K}^{-1}$]	1066	1092
Pr_L [-]	3.35	3.29
Pr_V [-]	0.885	0.888
σ [N m^{-1}]	0.0074	0.0061
p_r [-]	0.190	0.225

Among the listed properties, R134a shows a lower vapor density than R513A, i.e., at constant mass velocity the vapor velocity is higher, with consequent higher convective effects. Furthermore, the liquid thermal conductivity of R134a is higher than that of R513A, with consequently better thermal characteristics of the liquid film thickness. Considering the pressure drop, the higher vapor velocity at constant mass velocity for R134a will also be reflected in the hydraulic behavior.

Figure 9 shows a comparison between R134a and R513A heat transfer coefficient during condensation inside the microfin tube. As it appears from the figure, the heat transfer coefficients of R134a are higher than those of R513A, especially in the high vapor quality region, due to the aforementioned motivations. Similar conclusions can be drawn at a saturation temperature of 40 °C.

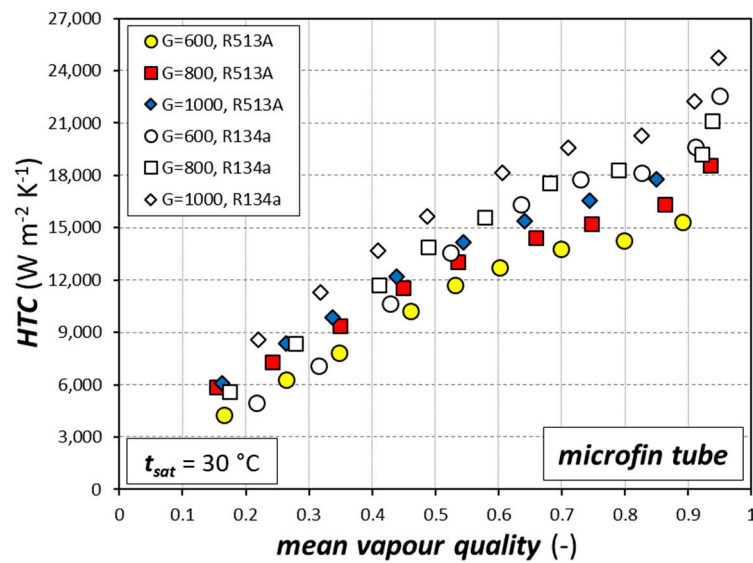


Figure 9. R134a and R513A heat transfer coefficient during condensation for the microfin tube vs. mean vapor quality at $t_{sat} = 30\text{ °C}$. G expressed in $[\text{kg m}^{-2} \text{s}^{-1}]$.

Frictional pressure gradients can be evaluated from the total measured pressure drop by subtracting the momentum pressure gradient. The model of Rouhani and Axelsson [27] is applied to estimate the void fraction, needed for the calculation of the momentum term. Figure 10 shows the comparison of frictional pressure gradients at $t_{sat} = 30\text{ °C}$. The frictional pressure gradient increases as the mass velocity increases and as the mean vapor quality increases, until a maximum value is reached at mean vapor qualities in the range 0.8–0.9, and then it slightly decreases. The comparison between the two fluids reveals that R134a shows a slightly higher frictional pressure gradient, especially at high vapor qualities, due to its lower vapor density with the consequent higher vapor velocity at constant mass velocity. A similar conclusion can be drawn at a saturation temperature of 40 °C .

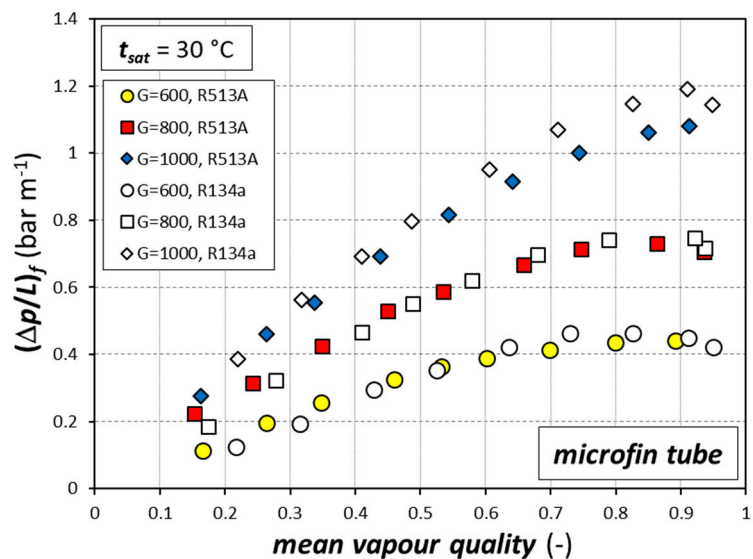


Figure 10. R134a and R513A frictional pressure gradient for the microfin tube vs. mean vapor quality at $t_{sat} = 30\text{ °C}$. G expressed in $[\text{kg m}^{-2} \text{s}^{-1}]$.

5. Empirical Modelling

5.1. Smooth Tube

This section provides a comparison between the experimental condensation heat transfer coefficients collected for the smooth tube and the values estimated by empirical correlations available in the literature. Figure 11 shows a comparison between the experimental heat transfer coefficients for the smooth tube and the values estimated by the correlations developed by Dobson and Chato [28], Shah [29], Cavallini et al. [30], and Dorao and Fernandino [31]. The correlation of Dobson and Chato [28] is able to estimate the experimental values with a relative deviation of 29.6%, an absolute deviation of 29.6%, and a standard deviation of 16.2%; the correlation of Shah [29] with a relative deviation of 16.3%, an absolute deviation of 18.0%, and a standard deviation of 18.4%; the correlation of Cavallini et al. [30] with a relative deviation of 5.9%, an absolute deviation of 9.7%, and a standard deviation of 13.6%; the correlation of Dorao and Fernandino [31] with a relative deviation of 2.5%, an absolute deviation of 15.3%, and a standard deviation of 22.8%. Therefore, the comparison reveals that the correlation of Cavallini et al. [30], even if it was developed for internal diameters larger than 3 mm, as well as that by Dorao and Fernandino [31], are the ones that better predict the experimental values.

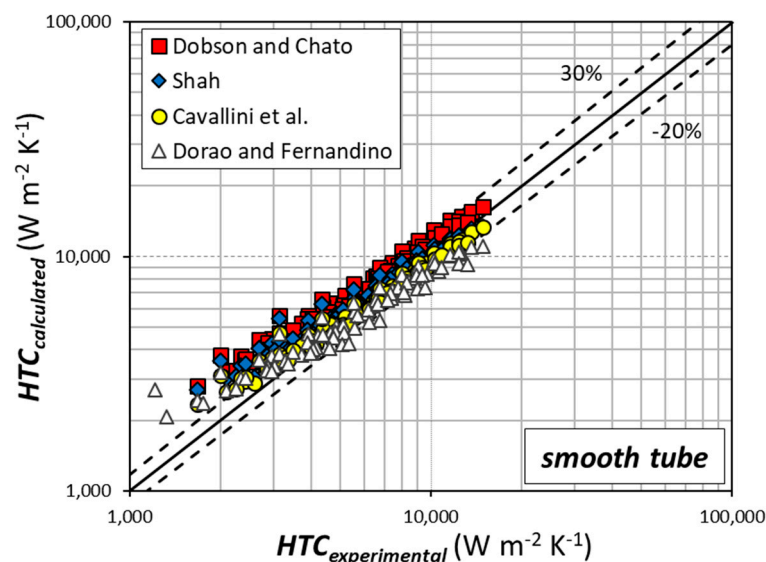


Figure 11. Experimental and calculated heat transfer coefficients for the 2.5 mm ID smooth tube. Models developed by Dobson and Chato [28], Shah [29], Cavallini et al. [30], and Dorao and Fernandino [31].

5.2. Microfin Tube

This section shows the comparison between the condensation heat transfer coefficients for the microfin tube against the values predicted by the correlation developed by Cavallini et al. [26]. A comparison between experimental and calculated condensation heat transfer coefficients is reported in Figure 12. The correlation can predict the experimental values with a relative, absolute, and standard deviation of 3.5%, 21.2%, and 31.1%, respectively. This correlation was developed from data obtained during condensation, for mass velocity in the range 80–890 kg m⁻² s⁻¹, saturation temperature in the range –15 °C–70 °C, inside microfin tubes with inner diameters at the fin tip from 5.9 mm and 14.2 mm. This aspect may partly explain the reason why the correlation tends to underestimate the experimental values at the lowest mass velocities in the high vapor quality zone, whose trend is peculiar of small-sized microfin tubes.

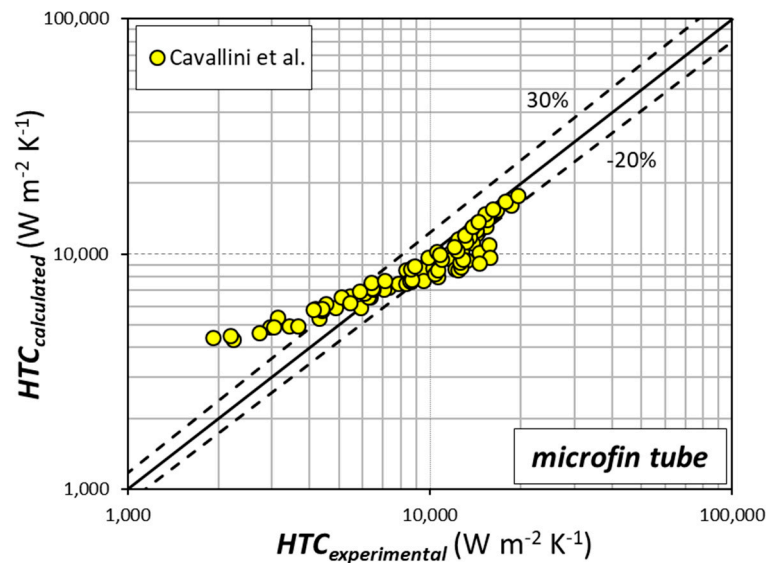


Figure 12. Experimental and calculated heat transfer coefficients for the 2.4 mm ID microfin tube. Model developed by Cavallini et al. [26].

6. Conclusions

The paper presented experimental data during condensation of R513A inside a smooth minitube with an inner diameter of 2.5 mm and inside a mini microfin tube with an inner diameter at the fin tip of 2.4 mm. The following working conditions were investigated: mass velocities in the range 200–1000 $\text{kg m}^{-2} \text{s}^{-1}$ and saturation temperatures at the inlet of the test section of 40 °C and 30 °C.

The test section for the smooth tube was verified during single-phase tests, involving liquid forced convection: once the heat flow rate calculated on the water side and the one on the refrigerant side were verified to be within $\pm 4\%$, and once the experimental heat transfer coefficients were found to be well estimated by correlations from the literature, the new test section was deemed verified.

The condensation tests revealed that the heat transfer coefficient increases as both vapor quality and mass velocity increases, both for the smooth tube and for the microfin tube. However, the increase of the heat transfer coefficient with vapor quality is more evident with the microfin tube at mass velocities up to 400 $\text{kg m}^{-2} \text{s}^{-1}$, highlighting its better convective properties, in particular at the lowest mass velocities. Concerning the saturation temperature, the higher the saturation temperature, the lower the heat transfer coefficient, for both the smooth tube and the microfin tube.

The average Enhancement Factor, i.e., the ratio between the heat transfer coefficient of the smooth tube and the one of the microfin tube under the same operative conditions, is 1.79, with the highest values shown at $G = 300 \text{ kg m}^{-2} \text{s}^{-1}$ at high vapor quality.

Experimental R513A heat transfer coefficients and frictional pressure drops obtained for the microfin tube were compared against the counterpart with R134a. R134a shows higher values of condensation heat transfer coefficient, particularly at high vapor qualities, but also slightly higher values of frictional pressure gradients.

The comparison against values predicted by empirical correlations revealed that the correlation of Cavallini et al. [30] and Dorao and Fernandino [31] are the most suitable to predict the condensation heat transfer coefficient inside the smooth tube, and the correlation of Cavallini et al. [26] is suitable to predict the condensation values for the microfin tube.

Author Contributions: Conceptualization, A.D.; validation, A.D.; investigation, A.D.; writing—original draft preparation, A.D.; visualization, A.D.; supervision, L.R.; funding acquisition, L.R. All authors have read and agreed to the published version of the manuscript.

Funding: This research was funded by MIUR through PRIN Project 2017F7KZWS_005 and by Università degli Studi di Padova through Project CPDA107382 and Project BIRD172935/17.

Acknowledgments: Jacopo Carnio is gratefully acknowledged.

Conflicts of Interest: The authors declare no conflict of interest.

Nomenclature

A	area [m ²]
c	specific heat [J kg ⁻¹ K ⁻¹]
D	diameter [m]
G	mass velocity [kg m ⁻² s ⁻¹]
h	specific enthalpy [J kg ⁻¹]
HTC	heat transfer coefficient [W m ⁻² K ⁻¹]
L	length [m]
\dot{m}	mass flow rate [kg s ⁻¹]
p	pressure [bar]
q	heat flow rate [W]
Pr	Prandtl number [-]
t	temperature [°C]
x	thermodynamic vapor quality [-]
Greek symbols	
Δp	pressure drop [Pa]
ΔT	temperature difference [K]
λ	thermal conductivity [W m ⁻¹ K ⁻¹]
μ	dynamic viscosity [Pa s]
ρ	density [kg m ⁻³]
σ	surface tension [N m ⁻¹]
Subscripts	
f	frictional
i	inner
in	at the inlet
L	of the saturated liquid
out	at the outlet
PC	at the pre-condenser
r	reduced
ref	of the refrigerant
sat	saturated
TS	in the test section
V	of the saturated vapor
vs	of the superheated vapor
w	of the water
$wall$	at the wall

References

- Hodnebrog, O.; Etminiam, M.; Fuglestedt, J.S.; Marston, G.; Myhre, G.; Nielsen, C.J.; Shine, K.P.; Wallington, T.J. Global warming potentials and radiative efficiencies of halocarbons and related compounds: A comprehensive review. *Rev. Geophys.* **2013**, *51*, 300–378. [[CrossRef](#)]
- Matkovic, M.; Cavallini, A.; Del Col, D.; Rossetto, L. Experimental study on condensation heat transfer inside a single circular minichannel. *Int. J. Heat Mass Transf.* **2009**, *52*, 2311–2323. [[CrossRef](#)]
- Zhang, H.Y.; Li, M.J.; Liu, N.; Wang, B.X. Experimental investigation of condensation heat transfer and pressure drop of R22, R410A and R407C in mini.tubes. *Int. J. Heat Mass Transf.* **2012**, *55*, 3522–3532. [[CrossRef](#)]
- Guo, Q.; Li, M.; Gu, H. Condensation heat transfer characteristics of low-GWP refrigerants in a smooth horizontal mini tube. *Int. J. Heat Mass Transf.* **2018**, *126*, 26–38. [[CrossRef](#)]
- Azzolin, M.; Bortolin, S.; Del Col, D. Convective condensation at low mass flux: Effect of turbulence and tube orientation on the heat transfer. *Int. J. Heat Mass Transf.* **2019**, *144*, 118646. [[CrossRef](#)]

6. Azzolin, M.; Berto, A.; Bortolin, S.; Moro, L.; Del Col, D. Condensation of ternary low GWP zeotropic mixtures inside channels. *Int. J. Refrig.* **2019**, *103*, 77–90. [[CrossRef](#)]
7. Murphy, D.L.; Macdonald, M.P.; Mahvi, A.J.; Garimella, S. Condensation of propane in vertical minichannels. *Int. J. Heat Mass Transf.* **2019**, *137*, 1154–1166. [[CrossRef](#)]
8. Gao, L.; Honda, T.; Koyama, S. Experiments on flow boiling heat transfer of almost pure CO₂ and CO₂-oil mixtures in horizontal smooth and microfin tube. *HVAC&R* **2007**, *13*, 415–425.
9. Kim, Y.J.; Cho, J.M.; Kim, M.S. Experimental study on the evaporative heat transfer and pressure drop of CO₂ flowing upward in vertical smooth and micro-fin tubes with the diameter of 5 mm. *Int. J. Refrig.* **2008**, *31*, 771–779. [[CrossRef](#)]
10. Dang, C.; Haraguchi, N.; Hihara, E. Flow boiling heat transfer of carbon dioxide inside a small-sized microfin tube. *Int. J. Refrig.* **2010**, *33*, 655–663. [[CrossRef](#)]
11. Qu, W.; Mudawar, I. Measurement and correlation of critical heat flux in two-phase micro.channel heat sinks. *Int. J. Heat Mass Transf.* **2004**, *47*, 2045–2059. [[CrossRef](#)]
12. Diani, A.; Campanale, M.; Cavallini, A.; Rossetto, L. Low GWP refrigerants condensation inside a 2.4 mm ID microfin tube. *Int. J. Refrig.* **2018**, *86*, 312–321. [[CrossRef](#)]
13. Bashar, M.K.; Nakamura, K.; Kariya, K.; Miyara, A. Experimental study of condensation heat transfer and pressure drops inside a small diameter microfin and smooth tube at low mass flux condition. *Appl. Sci.* **2018**, *8*, 2146. [[CrossRef](#)]
14. Diani, A.; Cavallini, A.; Rossetto, L. R1234yf flow boiling heat transfer inside a 2.4 mm microfin tube. *Heat Transf. Eng.* **2017**, *38*, 303–312. [[CrossRef](#)]
15. Jige, D.; Inoue, N. Flow boiling heat transfer and pressure drop of R32 inside 2.1 mm, 2.6 mm and 3.1 mm microfin tubes. *Int. J. Heat Mass Transf.* **2019**, *123*, 566–573. [[CrossRef](#)]
16. Hirose, M.; Jige, D.; Inoue, N. Optimum fin geometries on condensation heat transfer and pressure drop of R1234ze(E) in 4 mm outside diameter horizontal microfin tubes. *Sci. Technol. Built Environ.* **2019**, *25*, 1271–1280. [[CrossRef](#)]
17. Heredia-Aricapa, Y.; Belman-Flores, J.M.; Mota-Babiloni, A.; Serrano-Arellano, J.; Garcia-Pablon, J.J. Overview of low GWP mixtures for replacement of HFC refrigerants: R134a, R404A and R410A. *Int. J. Refrig.* **2020**, *111*, 113–123. [[CrossRef](#)]
18. Kedzierski, M.A.; Lin, L.; Kang, D. Pool boiling of low-global warming potential replacements for R134a on a reentrant cavity surface. *J. Heat Transf.* **2018**, *140*, 121502. [[CrossRef](#)]
19. Diani, A.; Rossetto, L. R513A flow boiling heat transfer inside horizontal smooth tube and microfin tube. *Int. J. Refrig.* **2019**, *107*, 301–314. [[CrossRef](#)]
20. Diani, A.; Rossetto, L. Characteristics of R513A evaporation heat transfer inside small-diameter smooth and microfin tubes. *Int. J. Heat Mass Transf.* **2020**, *162*, 120402. [[CrossRef](#)]
21. Lemmon, E.W.; Huber, M.L.; McLinden, M.O. *NIST Standard Reference Database 23, NIST Reference Fluid Thermodynamic and Transport Properties, REFPROP, Version 10.0, Standard Reference Data Program*; National Institute of Standards and Technology: Gaithersburg, MD, USA, 2018.
22. Kline, S.J.; McKlintock, F.A. Describing the uncertainties ins single-sample experiments. *Mech. Eng.* **1953**, *75*, 3–8.
23. Dittus, F.W.; Boelter, L.M.K. Heat transfer in automotive radiators of the annular type. *Univ. Calif. Publ. Eng.* **1930**, *2*, 443–461.
24. Petukhov, B.S.; Popov, V.N. Theoretical calculation of heat exchange and frictional resistance in turbulent flow in tubes of an incompressible fluid with variable physical-properties. *High Temper.* **1963**, *1*, 69–83.
25. Doretto, L.; Fantini, F.; Zilio, C. Flow patterns during condensation of three refrigerants: Microfin tube vs. smooth tube. In *Proceeding of the IIR International Conference on Thermophysical Properties and Transfer Processes pf Refrigerant*, Vicenza, Italy, 31 August–2 September 2005.
26. Cavallini, A.; Del Col, D.; Mancin, S.; Rossetto, L. Condensation of pure and near-azeotropic refrigerants in microfin tubes: A new computational procedure. *Int. J. Refrig.* **2009**, *32*, 162–174. [[CrossRef](#)]
27. Rouhani, S.Z.; Axelsson, E. Calculation of void fraction in the subcooled and boiling region. *Int. J. Heat Mass Transf.* **1970**, *13*, 383–393. [[CrossRef](#)]
28. Dobson, M.K.; Chato, J.C. Condensation heat transfer inside smooth horizontal tubes. *J. Heat Transf. ASME* **1998**, *120*, 193–213. [[CrossRef](#)]

29. Shah, M.M. An improved and extended general correlation for heat transfer during condensation in plain tubes. *HVAC&R Res.* **2009**, *15*, 889–913.
30. Cavallini, A.; Del Col, D.; Doretti, L.; Matkovic, M.; Rossetto, L.; Censi, G. Condensation in horizontal smooth tubes: A new heat transfer model for heat exchanger design. *Heat Transf. Eng.* **2006**, *27*, 31–38. [[CrossRef](#)]
31. Dorao, C.A.; Fernandino, M. On the heat transfer deterioration during condensation of binary mixtures. *Appl. Phys. Lett.* **2019**, *114*, 171902. [[CrossRef](#)]



© 2020 by the authors. Licensee MDPI, Basel, Switzerland. This article is an open access article distributed under the terms and conditions of the Creative Commons Attribution (CC BY) license (<http://creativecommons.org/licenses/by/4.0/>).